

Influence of Stretching Ratio and Salt Concentration on the Porosity of Polypropylene Films Containing Sodium Chloride Particles

Sven Sangerlaub,^{1,2} Maik Bohmer,³ Cornelia Stramm¹

¹Fraunhofer IVV Institute for Process Engineering and Packaging, Giggenhauser Strae 35, Freising, Germany

²TU Muenchen, Chair for Food Packaging Technology, Weihenstephaner Steig 22, Freising, Germany

³HTWK Leipzig, Faculty of Media, Karl-Liebknecht-Str. 145, Leipzig, Germany

Correspondence to: S. Sangerlaub (E-mail: sven.saengerlaub@ivv.fraunhofer.de)

ABSTRACT: The incorporation of salt in a polymer matrix could potentially achieve a humidity-regulating film system of high porosity for packaging applications. In this study, sodium chloride (NaCl) powder was used as a model substance for humidity-regulating fillers in polypropylene films. A polypropylene homopolymer was extrusion-blended with NaCl at concentrations of 0.03, 0.06, 0.12, and 0.24 g NaCl-g film⁻¹. Films were produced and were subsequently oriented mono and biaxially. At stretching ratios (SRs) of between 2 and 25 a porosity of 20% v/v to 50% v/v was achieved. The porosity positively correlated with the SR. An empirical model based on ellipsoids that approximated the correlation between the SR and the porosity was developed. This correlation offers a basis for further studies on other salt-polymer systems that have undergone differing orientation processes. © 2012 Wiley Periodicals, Inc. *J. Appl. Polym. Sci.* 129: 1238–1248, 2013

KEYWORDS: Active packaging; stretching ratio; micro-porous polypropylene film; sodium chloride; humidity-regulation

Received 8 July 2012; accepted 30 October 2012; published online 27 November 2012

DOI: 10.1002/app.38793

INTRODUCTION

Humidity-regulating Films with Salt Particles as Active Substances

One strategy to functionalize films is to blend active substances into their polymer matrix before film extrusion.¹ When a hygroscopic salt is used as an additive, for instance, a humidity-regulating polymer structure is achieved.² The resulting film absorbs water vapor when the relative humidity (RH) in the environment is higher than the equilibrium RH of the polymer-salt-structure and, contrarily, desorbs water vapor when the RH in the environment is below this equilibrium RH. Depending on the equilibrium RH and the sorption properties of the used salt, a salt solution can be formed during water vapor absorption. This liquid has a higher volume than the dry salt itself. However, to avoid migration of the salt solution it needs to be immobilized by the polymer matrix. One possibility to achieve this is the creation of porous polymer structures with closed capillaries, which could be generated by stretching (orientation) of salt-containing films. During orientation processes, salt particles induce capillary formation in the respective carrier polymer matrix,^{1,3,4} resulting in a structure with salt particles at the centre of the capillaries. During water vapor absorption a salt solution is formed in these capillaries (Figure 1).⁵ If the polymer matrix is impermeable for salt ions, this salt solution is

immobilized and its migration is prevented. In this case, only water vapor can permeate through the polymer matrix. To achieve these conditions a specific capillary headspace volume (cavity volume) or porosity of polymer matrix is required to provide sufficient space for the salt solution.

Generation of Porous Polymer Structures by Orientation

Wu et al. give an excellent overview of production and properties of micro-porous films.⁶ Stress-cracking during orientation of polymer structures with dispersed particles causes formation of micro-pores. The particles used should therefore be incompatible with the polymer matrix to achieve such effects. Several patents and publications describe the production of micro-porous films.^{3,6–15} In the case of an open-porous polymer structure the water vapor transmission rate increases.⁶ Wu et al. reported that the water vapor transmission rate of oriented polyethylene films rises dramatically when they are filled with more than 40% w/w calcium carbonate particles.⁶ This result indicates that below that filler content the pores are closed and are not interconnected. The porosity determines how much water vapor can be absorbed and stored in the capillaries by hygroscopic salts, even though the absorption capacity of a salt itself is an independent property that depends on its water vapor sorption isotherm. This assertion is based on the assumption that exceeding the limit for water vapor absorption

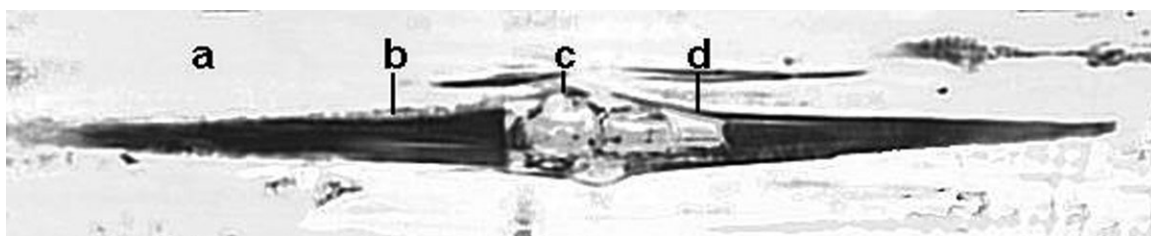


Figure 1. Microscopic picture; side view of monoaxially-oriented PP-film with NaCl particles stored at 100% RH and 23°C; (a) polymer matrix, (b) capillary, (c) NaCl particle, (d) salt solution.⁵

determined by porosity leads to a pressure increase in the capillary system. Consequently, a salt solution is released by the capillaries if the polymer matrix is stress-cracked due to pressure enhancement.

Properties of Polypropylene (PP) Relevant for Orientation

When used as a polymer matrix, PP is characterized by its high stretchability, which shows stretching ratios (SRs) of between 5 and 9 in the *x* and *y*-directions in biaxial orientation at temperatures of between 140°C and 160°C.¹⁶

During orientation, PP films are heated to temperatures ranging between 120°C and 160°C.¹⁷ PP has a higher specific volume at higher temperatures. Domininghaus reported a specific volume of PP homopolymer of circa 1.1 cm³·g⁻¹ at 23°C and circa 1.2 cm³·g⁻¹ at 160°C.¹⁸ The linear thermal expansion coefficient of PP is reported to be 1.05·10⁻⁴ K⁻¹ at 23°C and 2.2·10⁻⁴ K⁻¹ at 110°C.¹⁸ In PP, like in other polymers, the Poisson effect occurs. When PP is stretched in one direction it tends to distort in the two other directions. The Poisson effect is characterized by Poisson's ratio μ and is defined as the quotient from the change in width per unit width and change in length per unit length.^{19,20} At a Poisson's ratio of 0.5 the volume does not change under strain.²¹ Saechtling reported a Poisson's ratio for PP of 0.34 at 20°C and 0.47 at 90°C.²¹

Intention of the Present Study

Porosity characteristics of PP and other polymer matrices after salt addition are scarcely available in the literature. The aim of the present study was therefore to investigate the influences of the SR and sodium chloride (NaCl) concentration on the porosity of the resulting PP films. Different NaCl concentrations

and particle sizes were used. Porosity was determined via density measurements. Furthermore, porosity was calculated using a mathematical model based on ellipsoids. The derivation of the model considers (1) the size of the pores, which were calculated and measured from microscopic images and (2) the SRs of the respective films. The results should facilitate the adjustment of porosity of films by orientation processes by taking into account the influence of salt concentration and the SR in the model. The correlation found might serve as a basis for further studies on other salt-polymer systems that have undergone differing orientation processes under different orientation conditions and for application to various polymer matrices.

EXPERIMENTAL

Experimental Plan

PP films containing 0.03, 0.06, 0.12, and 0.24 g NaCl·g film⁻¹ with particle sizes [volume median diameter; *D*(*v*, 0.5)] of 8 μm, 30 μm, and 91 μm were produced. These were oriented (stretched) by applying different stretching processes, i.e. monoaxial, biaxial-simultaneous and biaxial-sequential orientation. Different SRs were applied. Porosities of the resulting films were calculated (1) from their measured density and correlated with the SR and (2) by applying a model based on ellipsoids that included SR and salt concentration. SRs were drawn from the laboratory stretching machine for the specific orientation applied. Capillary sizes were measured from microscopic images. Porosity data obtained from the two methods were compared. The model was adapted using experimental results. Additionally, the influence of particle size on porosity was studied. Table I shows the samples produced for the experiments.

Table I. Summary of Production Parameters for PP Film Samples

ASR	2	3	4	5	6	9	16	25
Monoaxial orientation								
0, 0.03, 0.06, 0.12, 0.24 g NaCl·g film ⁻¹ ; <i>D</i> (<i>v</i> , 0.5): 30 μm	x	x	x	x	x			
0.06 g NaCl·g film ⁻¹ ; <i>D</i> (<i>v</i> , 0.5): 8 μm and 91 μm			x					
Biaxial orientation								
(SR in <i>x</i> -axis and in <i>y</i> -axis)	(1.41-1.41)		(2-2)			(3-3)	(4-4)	(5-5)
Biaxial-simultaneous orientation								
0, 0.03, 0.06, 0.12, 0.24 g NaCl·g film ⁻¹ ; <i>D</i> (<i>v</i> , 0.5): 30 μm	x		x			x	x ^a	x
0.06 g NaCl·g film ⁻¹ ; <i>D</i> (<i>v</i> , 0.5): 8 μm and 91 μm						x		
Biaxial-sequential orientation								
0.03, 0.06 g NaCl·g film ⁻¹ ; <i>D</i> (<i>v</i> , 0.5): 30 μm	x		x			x	x	x

^aOnly 0.06.

Definitions. In this article the SR of a film in the x or y -direction is defined as the ratio of length after orientation, l_{oriented} , and length before orientation, $l_{\text{non-oriented}}$, in the respective direction (eq. 1).

$$SR = \frac{l_{\text{oriented}}}{l_{\text{non-oriented}}} \quad (1)$$

The area stretching ratio (ASR) is defined as the ratio of the area after orientation, A_{oriented} , and before orientation, $A_{\text{non-oriented}}$ (eq. 2).

$$ASR = \frac{A_{\text{oriented}}}{A_{\text{non-oriented}}} \quad (2)$$

The ASR is the product of SR in the x and y -directions (eq. 3). In the case of mono-axial orientation, ASR approximates to SR. Poisson's effect at higher SR in one direction results in a higher vertical thinning of ellipsoids (see RESULTS AND DISCUSSION and Table 3).

$$ASR = SR_{x\text{-axis}} \cdot SR_{y\text{-axis}} \quad (3)$$

NaCl. NaCl (Siedepfeisesalz extrafein; esco-european salt company GmbH&CO. KG; Hannover, Germany) with $10 \text{ mg}\cdot\text{kg}^{-1}$ of the release agents E535 and E536 was used as a model substance.²² The density of NaCl is $2.17 \text{ g}\cdot\text{cm}^{-3}$.²³

Micronization of NaCl. NaCl with a particle size of $D(v, 0.5)$ $8.4 \mu\text{m}$ (sample 1) was produced in a fluidized bed-opposed jet mill (AFG 200; Hosokawa Alpine AG; Augsburg, Germany). NaCl with a particle size of $D(v, 0.5)$ $30.1 \mu\text{m}$ (sample 2) was manufactured using an alternative fluidized bed-opposed jet mill (MultiNo[®] 2000; Schüttgutveredelung NOLL GmbH; Bobingen, Germany). NaCl with a particle size of $D(v, 0.5)$ $91.0 \mu\text{m}$ (sample 3) was gained by sieving NaCl in a screening machine (Vibro; Retsch GmbH; Haan Germany) using two sieves (Retsch GmbH; Haan, Germany) with mesh openings of $63 \mu\text{m}$ and $100 \mu\text{m}$, respectively.

Particle Size Distribution of NaCl. Particle sizes (volume diameter) were calculated from particle volume distribution measurements. The median volume diameter $D(v, 0.5)$ is defined as the diameter where 50% v/v of the particle amount is below and 50% v/v is above that value.²⁴ Since NaCl powder was milled or sieved at different production sites, particle sizes were determined using the respective on-site testing devices as follows: (1) Particle size distributions of NaCl samples 1, 2, and 3 were measured with a laser diffraction-based system (Mastersizer S long bench; Malvern Instruments GmbH; Herrenberg, Germany) using a wet dispersion unit and 1-butanol p.a. (VWR, Germany) as the dispersion medium (Mastersizer; Malvern Instruments GmbH; Herrenberg, Germany). The system parameters applied were: software version 15.1, lens 300RF ($0.05\text{--}900 \mu\text{m}$), wet dispersion unit MS 1, beam length 2.4 mm , Mie theory with optical parameters for particles $R.I. = 1.5295$, 0.1000 , and dispersion medium $R.I. = 1.3300$ (software code 3OHD), analysis model polydisperse, repeat determination, dispersion time $2\text{--}3 \text{ min}$, non-ultrasound, stirrer speed 3000 rpm . (2) Particle size distribution of sample 1 was measured using a second method based on laser diffraction (Sympatec Helos (H0174) Rodos; Sympatec GmbH; Clausthal-Zellerfeld,

Germany) under dry conditions. The parameters were: pressure 2 bar , negative pressure 78 mbar , conveying rate 30% , bed height 2 mm , measuring conditions standard Rodos 0.1, measuring range R4: $0.5/1.8\text{--}350 \mu\text{m}$, measuring time 10 s , evaluation HRLD (V 3.4 Rel.1). (3) Sample 2 was measured via a third method based on laser diffraction (Cilas 920; Cilas; Orleans, France). The parameters applied were: liquid isopropyl alcohol, dispersing agent propanol, ultrasound 60 s (+M.) , concentration 166 . Due to the fact that all tests with the "Mastersizer" were carried out under the same conditions, systematic errors should be the same throughout these results.

Polypropylene. A polypropylene homopolymer (HP 525 J; LyondellBasell; Rotterdam, The Netherlands) designed for biaxially-oriented PP films (PP-BO) was used. This polymer did not contain slip agents, anti-blocking agents or calcium stearate.²⁵ The density was $0.90 \text{ g}\cdot\text{cm}^{-3}$. The crystallite melting point was 170°C , as measured with differential scanning calorimetry (model 821; Mettler Toledo; Gießen, Germany) at a heating rate of 10°C per minute. A SR of 7×7 at a temperature of 150°C is given in the product data sheet, which is below the crystallite melting temperature of PP.

Sample Production

A master batch with NaCl $D(v, 0.5)$ $30.1 \mu\text{m}$ with $0.6 \text{ g NaCl}\cdot\text{g}^{-1}$ master batch was produced on a twin screw extruder by Gabriel-Chemie (Weitnau, Germany). Compounds of NaCl with $D(v, 0.5)$ of $8.4 \mu\text{m}$ and $91 \mu\text{m}$ were produced by Fraunhofer IVV (Freising, Germany) using a Leistritz twin screw extruder (LSM 34 GL/GG; Leistritz AG; Nürnberg, Germany). The polymer strands were water-cooled and subsequently pelletized by a pelletizer (SGS 50E, C.F.; Scheer&CIE GmbH&Co. KG; Stuttgart, Germany). Compounds and PP without NaCl ribbons were extruded from the master batch on the same Leistritz twin screw extruder equipped with a slit die. The applied rotation speed was 50 rpm , and temperatures of the heating zones were between 100°C and 220°C . The ribbons were cooled with water.

Pressing to Films

The ribbons were pressed to films using a heated plate press (Type 341-50-12x12; Loomis products Kahlefeld GmbH; Kahlefeld, Germany) at a temperature of 200°C and at pressures of between 20 kN and 30 kN . Bar spacers with a thickness of $800 \mu\text{m}$ were used to adjust the thickness of non-oriented films to around $800 \mu\text{m}$.

Orientation

PP films with and without incorporated NaCl with a length and width of 85 mm were mono-axially, biaxial-simultaneous and biaxial-sequentially oriented with a laboratory stretching machine (Karo IV; Brückner Maschinenbau GmbH & Co. KG; Siegsdorf, Germany). The films were heated for 50 s at 145°C before orientation. The orientation velocity was 400% per second.

Sampling for Microscopic Analysis

Sampling for microscopic analysis was conducted with biaxial-simultaneous orientated films with $0.06 \text{ g NaCl}\cdot\text{g film}^{-1}$; NaCl $D(v, 0.5)$ of $30.1 \mu\text{m}$. The analysis was done at three sites of the film for three capillaries each (Figure 2).

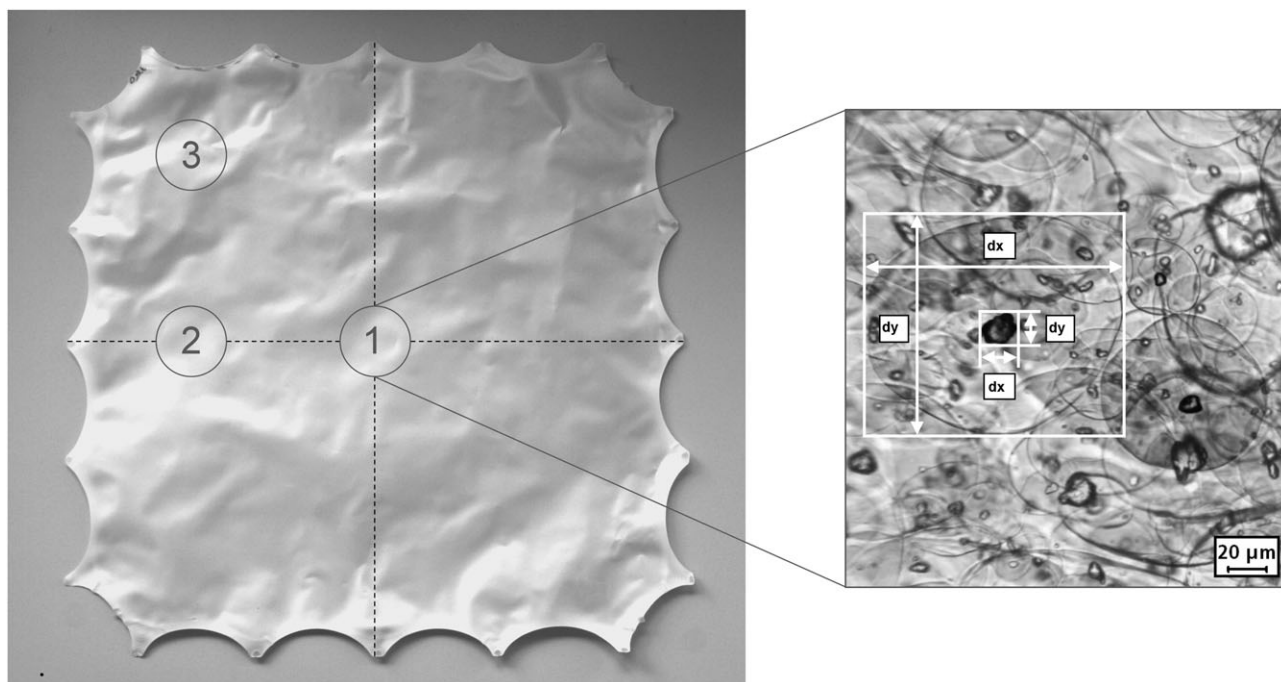


Figure 2. Schematic depiction of sampling sites for microscopic analysis.⁵

Theoretical Model for Porosity of Films

Porosity P is defined as the quotient from the volume of capillaries in a medium $V_{\text{headspace}}$, (headspace synonymous with cavity volume in this work), and the volume of medium, V_{medium} (eq. 4). The volume of a medium, V_{medium} , can be calculated when the density and weight of a medium are known. The volume of capillaries in a medium, $V_{\text{headspace}}$, per one gram of film can be calculated for porosity P by applying eq. (4).

$$P = \frac{V_{\text{headspace}}}{V_{\text{medium}}} \cdot 100\% \quad v/v \quad (4)$$

In case of a porous, filled polymer V_{medium} is the sum of (1) volume of capillaries $V_{\text{headspace}}$, (2) volume of polymer matrix V_{polymer} and (3) volume of filler V_{filler} (eq. 5).

$$V_{\text{medium}} = V_{\text{headspace}} + V_{\text{polymer}} + V_{\text{filler}} \quad (5)$$

Porosity P was calculated from the density of the non-oriented films containing NaCl particles, $\sigma_{\text{non-oriented}}$, and the density of oriented films containing voids with NaCl particles, σ_{oriented} , according to eq. (6),^{10,11} which was deducted from eq. (4). However, eq. (6) causes a systematic error because the density of the (carrier) polymer matrix may change during orientation processes. The error can be neglected when the density change of the polymer matrix is small, as is the case in this work (see results for density in “RESULTS AND DISCUSSION”).

$$P = \left(1 - \frac{\delta_{\text{oriented}}}{\delta_{\text{non-oriented}}} \right) \cdot 100\% \frac{V}{V} \quad (6)$$

The density of the films was measured by applying the Archimedes principle with a density determination kit for analytical balances

(Mettler-Toledo AG; Greifensee, Switzerland) and an analytical balance (AT261 DeltaRange[®]; Mettler-Toledo AG; Greifensee, Switzerland). Density of samples δ were measured according to eq. (7) at 20°C and calculated from the weight of the sample in air A and the weight of the sample in an auxiliary liquid (99.8% w/w ethanol, rest water, $\sigma_0 = 0.7893 \text{ g}\cdot\text{cm}^{-3}$) B .²⁶ Air density was neglected because of its minor influence on the results.

$$\delta = \frac{A}{A - B} \cdot \delta_0 \quad (7)$$

Thickness of Samples

The thickness of the samples was measured with a calliper (Solar-Absolute Digimatic Calliper; Mitutoyo Deutschland GmbH; Neuss, Germany), whereby 20 measuring points per sample were taken to determine a single thickness.

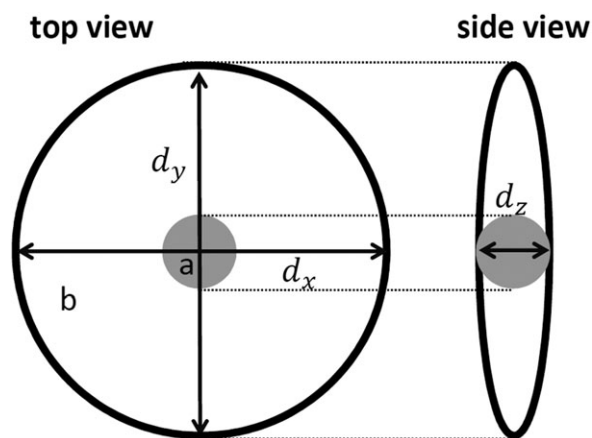
Optical Microscopy

A light microscope (LeitzDiaplan; Mikroskopie und Systeme GmbH;

Wetzlar, Germany) was used to determine the NaCl distribution in the polymer matrix and the cavity, as well as the NaCl dimensions. A thin piece was cut out of a sample and fixed on an objective plate using a transparent adhesive tape. The transmitted-light method was applied to analyse samples for particle distribution at 100 and 200 x magnifications.

Calculation of Confidence Intervals

Error bars in the following figures (“RESULTS and DISCUSSION”) show confidence intervals based on at least five measurement repetitions and a level of significance of 5%.²⁷



a: particle in the center of the ellipsoid

b: headspace of the ellipsoid

Figure 3. Schematic depiction of ellipsoid with particle (sphere) at centre.⁵

Ellipsoids

The volume, $V_{\text{ellipsoid}}$, of an ellipsoid can be calculated from its three diameters along the x , y , and z -axes (Figure 3, eq. 8).²⁸

$$V_{\text{ellipsoid}} = \frac{1}{6} \cdot \pi \cdot d_x \cdot d_y \cdot d_z \quad (8)$$

During orientation of filled polymers, the polymer matrix tears off the fillers to form capillaries. Assuming the boundary conditions that (1) particles are spheres with a diameter d_z centered in the middle of the capillaries, (2) the capillaries are ellipsoids with a diameter d_x and d_y , and (3) SR along the x -axis $SR_{x\text{-axis}}$ is $d_x \cdot d_z^{-1}$ (eq. 9) and along the y -axis is (eq. 10), the headspace volume of the capillaries can be calculated using eq. (8). (It should be noted that this approach neglects the Poisson effect, which causes a thinning of the capillaries. Although it is a good approximation at low SR, deviations at higher SR are greater. This point is addressed in “RESULTS and DISCUSSION”, section “Empiric model for headspace volume of capillaries”.)

$$SR_{x\text{-axis}} = \frac{dx}{dz} \quad (9)$$

$$SR_{y\text{-axis}} = \frac{dy}{dz} \quad (10)$$

Headspace Volume of a Stretched Film with Fillers. The headspace volume of the capillaries, $V_{\text{headspace,model ellipsoid}}$, of a filled film with uniform particle size is derived from the volume of a single ellipsoid, $V_{\text{ellipsoid}}$, the volume of one filler particle, V_{particle} , and the amount of particles in a film, n_{particle} (eq. 11).

$$V_{\text{headspace,ellipsoid}} = (V_{\text{ellipsoid}} - V_{\text{particle}}) \cdot n_{\text{particle}} \quad (11)$$

The volume of an ellipsoid is calculated according to eq. (8). In the case of homogenous biaxial orientation with equal SRs

along the x and y -axes, eqs. (9), (10), and (3) can be inserted into eq. (8) to form eq. (12).

$$V_{\text{ellipsoid}} = \frac{1}{6} \cdot \pi \cdot ASR \cdot d_z^3 \quad (12)$$

The volume, V_{particle} , of a spherical particle is calculated from its diameter (eq. 13).

$$V_{\text{particle}} = \frac{1}{6} \cdot \pi \cdot d_z^3 \quad (13)$$

The amount of filler particles, $n_{\text{headspace}}$, in a film is calculated from the volume of one particle, V_{particle} , and the volume of all particles, V_{filler} (eq. 14)

$$n_{\text{particles}} = \frac{V_{\text{filler}}}{V_{\text{particle}}} \quad (14)$$

The volume of all particles, V_{filler} , is calculated from its density, σ_{filler} , and weight, m_{filler} (eq. 15).

$$V_{\text{filler}} = \frac{m_{\text{filler}}}{\delta_{\text{filler}}} \quad (15)$$

The weight of the particles, m_{filler} , is calculated from the weight of the filled film containing the particles, $V_{\text{filled,film}}$, and the filling ratio y_{filler} (0 .. 1; 0: no filler; 1: 100% w/w filler) in film (eq. 16).

$$m_{\text{filler}} = m_{\text{filled film}} \cdot y_{\text{filler}} \quad (16)$$

Inserting eqs. (13), (15), and (16) into eq. (14) results in eq. (17).

$$n_{\text{particle}} = \frac{6 \cdot m_{\text{filled film}} \cdot y_{\text{filler}}}{\pi \cdot d_z^3 \cdot \delta_{\text{filler}}} \quad (17)$$

Inserting eqs. (12), (13), and (17) into eq. (11) leads to eq. (18).

$$V_{\text{headspace, ellipsoid}} = (ASR - 1) \cdot m_{\text{filled film}} \cdot \frac{y_{\text{filler}}}{\delta_{\text{filler}}} \quad (18)$$

According to eq. (18), $V_{\text{headspace}}$ of the capillaries of oriented films is dependent on ASR and filler content y_{filler} , but is independent of particle diameter. At constant filler content, $V_{\text{headspace}}$ increases linearly with ASR according to eq. (18). Expected deviations occurring due to the Poisson effect are addressed in “RESULTS and DISCUSSION”, section “Empiric model for headspace volume of capillaries”.

Porosity of a Stretched Film with Fillers. Equations (4) and (5) are used to calculate porosity P of oriented filled films. The volume of polymer matrix, V_{polymer} , is calculated from its density, σ_{polymer} , and weight, m_{polymer} (eq. 19).

$$V_{\text{polymer}} = \frac{m_{\text{polymer}}}{\delta_{\text{polymer}}} \quad (19)$$

The weight of the polymer, m_{polymer} , is calculated from the weight of the filled film, $m_{\text{filled film}}$, and the filling ratio at a

Table II. Particle Sizes of Used NaCl Powders Measured with Different Testing Devices; Underlined Values (Testing Device “Mastersizer”) Are Used as Reference Values in the Manuscript

	Particle size (volume diameter) [μm]			Testing device
	D(v, 0.1)	D(v, 0.5)	D(v, 0.9)	
Sample 1	1.7	8.4	55.0	“Mastersizer”
	0.7	1.6	3.0	“Sympatec”
Sample 2	8.6	30.1	58.0	“Mastersizer”
	2.2	13.8	31.0	“Cilas”
Sample 3	58.3	91.0	130.0	“Mastersizer”

polymer, γ_{filler} (eq. 20).

$$m_{\text{polymer}} = m_{\text{filled film}} - m_{\text{filled film}} \cdot \gamma_{\text{filler}} \quad (20)$$

Inserting eq. (20) into eq. (19) produces eq. (21).

$$v_{\text{polymer}} = \frac{m_{\text{filled film}} - m_{\text{filled film}} \cdot \gamma_{\text{filler}}}{\delta_{\text{polymer}}} \quad (21)$$

When eq. (16) is inserted into eq. (15) and the result is subsequently inserted with eqs. (18) and (21) into eqs. (5) and (22) results.

$$v_{\text{medium}} = \frac{m_{\text{filled film}} - m_{\text{filled film}} \cdot \gamma_{\text{filler}}}{\delta_{\text{polymer}}} + \frac{m_{\text{filled film}} \cdot \gamma_{\text{filler}}}{\delta_{\text{filler}}} + (ASR - 1) \cdot m_{\text{filled film}} \cdot \frac{\gamma_{\text{filler}}}{\delta_{\text{filler}}} \quad (22)$$

When eqs. (18) and (22) are inserted into eqs. (4) and (23) results.

$$P = \frac{ASR - 1}{\frac{\delta_{\text{filler}}}{\gamma_{\text{filler}} \cdot \delta_{\text{polymer}}} - \frac{\delta_{\text{filler}}}{\delta_{\text{polymer}}} + ASR} \cdot 100\% \frac{v}{V} \quad (23)$$

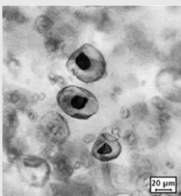
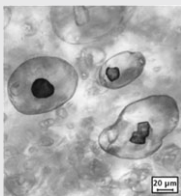
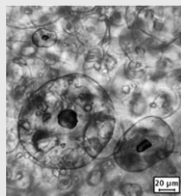
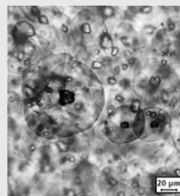
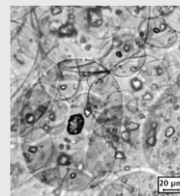
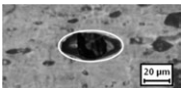
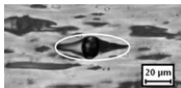
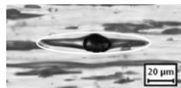
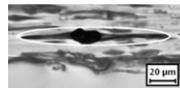
According to eq. (23), the porosity of an oriented filled film is dependent on the filler content, γ_{filler} and the area SR ASR, but is independent of the particle size of filler.

RESULTS AND DISCUSSION

Particle Size Distribution of NaCl

The milling and sieving of NaCl resulted in a distribution curve. Table II shows D(v, 0.1), D(v, 0.5) and D(v, 0.9) values for the three salts with different particle size distributions. Particle size measurements conducted with the “Sympatec” and the “Cilas” testing devices differed from the results with the “Mastersizer”

Table III. Microscopic Pictures of Biaxial-simultaneous Orientated Films with 0.06 g NaCl·g film⁻¹; D(v, 0.5) of NaCl 30.1 μm ; SR in x- and y-Axis from Microscopic Analysis⁵

Top view					
ASR ^a	2	4	9	16	25
SR in x-axis ^a	1.41	2	3	4	5
SR in y-axis ^a	1.41	2	3	4	5
Microscopic analysis					
SR _x	2.0 ± 0.4	3.2 ± 0.5	3.7 ± 0.5	5.0 ± 0.4	6.6 ± 0.8
SR _y	2.1 ± 0.4	3.5 ± 0.5	3.7 ± 0.7	5.1 ± 0.7	6.4 ± 1.0
Side view					
SR in x-axis ^a	1.41	2	3	4	
Microscopic analysis					
SR _x	1.9 ± 0.4	3.3 ± 1.0	4.1 ± 1.0	4.8 ± 1.4	

^aValues from stretching machine.

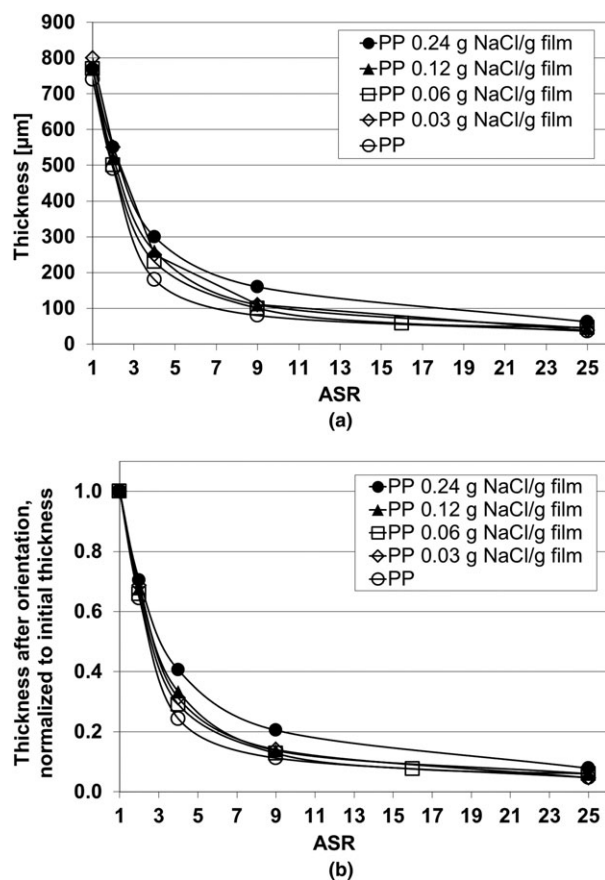


Figure 4. Thickness of films after orientation, biaxial-simultaneous orientated films; $D(v, 0.5)$ of NaCl $30.1 \mu\text{m}$.⁵

testing device. The “Mastersizer” produced higher $D(v, 0.1)$, $D(v, 0.5)$ and $D(v, 0.9)$ values. The particle diameters of NaCl particles (sample 2) in films were measured with a microscope (110 measurements) to analyze the SR for Table III and Figure 5. The medium particle size was $17.9 \mu\text{m}$ with a minimum diameter of $6.4 \mu\text{m}$ and a maximum diameter of $33.6 \mu\text{m}$. The results from the “Cilas” testing device were therefore in better agreement with the microscopic analysis than those of the “Mastersizer” tests. Differences in measured particle size distributions can be attributed to different measuring methods and the possible occurrence of agglomerates during the test with the “Mastersizer” testing device.

Thicknesses of Examined Films

The thickness of samples decreased with orientation, as expected [Figure 4(a,b)]. This result is in agreement with the findings of Nago et al.¹⁰ It was observed that the thickness decreased less at a higher salt content of the films, indicating that the porosity increased due to capillary formation during the orientation process. Poisson’s ratio can be calculated from the ratio of the thickness before and after orientation as a function of ASR. However, the authors found that the thickness of the samples varied too much to achieve reliable results for calculating Poisson’s ratio. The thickness of the films (minimum and maximum values) before orientation was between $670 \mu\text{m}$ and $860 \mu\text{m}$ for PP films, between $720 \mu\text{m}$ and $900 \mu\text{m}$ for PP films with 3 g

NaCl·g film⁻¹, between $700 \mu\text{m}$ and $920 \mu\text{m}$ for PP films with 6 g NaCl·g film⁻¹, between $680 \mu\text{m}$ and $910 \mu\text{m}$ for PP films with 12 g NaCl·g film⁻¹, and between $690 \mu\text{m}$ and $870 \mu\text{m}$ for PP films with 24 g NaCl·g film⁻¹ for $D(v, 0.5)$ of NaCl $30.1 \mu\text{m}$.

ASR and SR via Microscopic Analysis and Calculation

NaCl particles were torn off by the PP matrix by stress cracking during biaxial orientation (Table III). The resulting capillaries showed a smaller volume than the respective ellipsoids. Three effects may have caused these deviations: (1) the Poisson effect, causing a thinning of the capillaries, (2) contraction of PP at lower temperatures (see INTRODUCTION, section “generation of porous polymer structures by orientation”), and (3) a possible formation of a vacuum when capillaries are induced. These effects were not examined in this study. Therefore, the model ellipsoid needed to be adapted to describe the correlation between ASR and porosity. Furthermore, NaCl particles were not spherical in shape. The SR produced by the stretching machine was found to be lower than the SR measured from microscopic analysis (Figure 5). This result can be attributed to the shape of the non-spherical NaCl particles, which may have caused deviations in measuring the dimensions in the film. Furthermore, capillaries formed are like cracks in the matrix that propagate beyond the strain imposed. The accumulated strain energy is released due to the elastic component of the deformation.

Density

Orientation of PP leads to a slight increase in density. The mean density of non-oriented PP films without NaCl was $(0.907 \pm 0.001) \text{g}\cdot\text{cm}^{-3}$. The mean density of mono-axial orientated PP films without NaCl at a SR of 2, 4, and 6 increased to $(0.909 \pm 0.001) \text{g}\cdot\text{cm}^{-3}$ and the mean density of biaxial-simultaneous orientated films increased to $(0.909 \pm 0.002) \text{g}\cdot\text{cm}^{-3}$. The density increase was neglected in calculations of the porosity of oriented PP films with NaCl (eq. 6) due to its low value and correspondingly low error. Density values after orientation were drawn for calculation of the porosity of oriented films (eqs. 23 and 26). The density increase can be attributed to a higher alignment of polymer chains during orientation as a result of enhancement in the formation of polymer crystals,

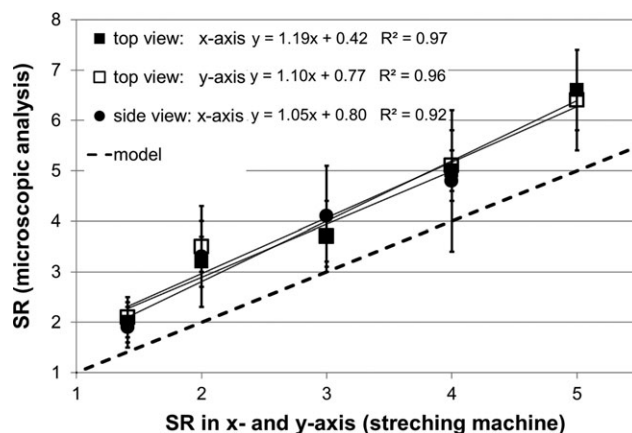


Figure 5. SR gained from microscopic analysis as a function of SR of stretching machine; biaxial-simultaneous orientated films with $0.06 \text{g NaCl}\cdot\text{g film}^{-1}$; $D(v, 0.5)$ of NaCl $30.1 \mu\text{m}$.⁵

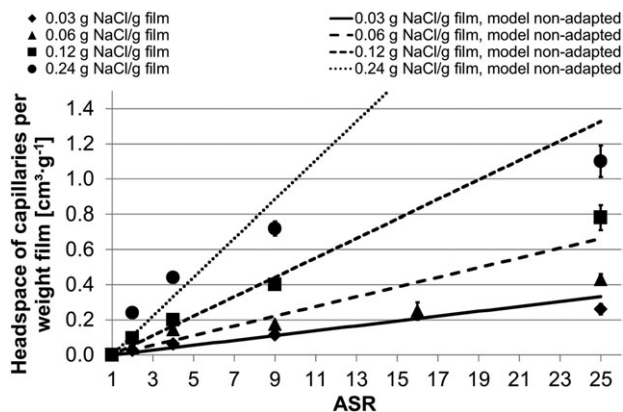


Figure 6. Headspace of capillaries per weight of film as a function of ASR; biaxial-simultaneous orientated films; D(v, 0.5) of NaCl 30.1 μm ; model non-adapted equation 18.⁵

which have a higher density than the amorphous phase.¹⁷ Furthermore, orientation reduces the free volume in the polymers, resulting in a better packing of polymer chains and crystallites. Additionally, higher temperatures favor crystallization of polymers.

Empiric Model for Headspace Volume of Capillaries

The headspace volume of capillaries per weight of film as a function of the ASR yields a linear correlation for the non-adapted model based on ellipsoids (eq. 18). However, the results showed a significant deviation from the model (Figure 6). To adapt the model, the measured headspace of capillaries in films, $V_{\text{headspace,measured}}$, was normalized to the respective calculated headspace of capillaries (eq. 18) assuming ideal ellipsoids, $V_{\text{headspace,model ellipsoids}}$ (Table IVa). If normalization leads to values of one, measured and calculated (model ellipsoid) values are equal.

Normalized values were plotted as function of the natural logarithm of ASR (Figure 7). The correlations for different NaCl contents in films were linear. The R » value, which describes the deviation from this linear fit, ranged between 0.93 and 0.96, except

for films with 6 g NaCl·g film⁻¹ where R » was 0.72. In the latter case a poor correlation with the linear fit was observed, the reasons for which are unclear. The average of the trends is calculated as, $V_{\text{headspace,measured}} \cdot V_{\text{headspace,model ellipsoid}}^{-1} = (2.1 - 0.49 \cdot \ln(\text{ASR}))$ thus $V_{\text{headspace,measured}} = (2.1 - 0.49 \cdot \ln(\text{ASR})) \cdot V_{\text{headspace,model ellipsoid}}$ (eq. 24). Equation 24 was applied to eq. (18) to give eq. (25) (adapted model). The measured headspace of the capillaries in the films, $V_{\text{headspace,measured}}$, were normalized to the calculated headspace of the capillaries, $V_{\text{headspace,model ellipsoid}}$ (eq. 25) by applying the adapted model (Table IVa). The deviation of the model ellipsoid and the adapted model was calculated (Table IVb). The deviation for all salt concentrations was reduced by half. For ASRs of 2 and 4 the deviation reduced most, i.e. by a factor of 5 and 3, respectively. The average deviation reduced from 0.45 (model ellipsoid) to 0.17 (adapted model). Therefore the adapted model was better suited than the model ellipsoid to approximate the headspace increase of capillaries as a function of ASR. However, the results show that the model needs to be more refined to approximate the behavior during orientation. With the adapted model (eq. 25) for $V_{\text{headspace,model ellipsoids}}$ eq. (26) (adapted model for porosity) was obtained from eq. (18) by following the same derivation as for eq. (23) (see “EXPERIMENTAL”, section “Calculation model for porosity of films”).

$$V_{\text{headspace,adapted}} = (\text{ASR} - 1) \cdot m_{\text{filled film}} \cdot \frac{\gamma_{\text{filler}}}{\delta_{\text{filler}}} \cdot (2.12 - 0.49 \cdot \ln(\text{ASR})) \quad (25)$$

$$P = \frac{(\text{ASR} - 1) \cdot (2.12 - 0.49 \cdot \ln(\text{ASR}))}{\frac{\gamma_{\text{filler}}}{\gamma_{\text{filler}} \cdot \delta_{\text{polymer}} - \delta_{\text{filler}} + 1 + (\text{ASR} - 1) \cdot (2.12 - 0.49 \cdot \ln(\text{ASR}))} \cdot 100\% \frac{v}{v} \quad (26)$$

The adapted model (eqs. 25 and 26) showed a better correlation with the experimental results (Figures 8, 9). However, divergences between the measured and calculated results still occurred. Therefore, the adapted model is suggested to approximate real porosities.

Orientation Process

Porosities of biaxial-simultaneous and biaxial-sequential orientated as well as of mono-axial and biaxial-simultaneous

Table IVa. Headspace Per Weight of Film Calculated from Measured Density Normalized to Calculated Values Using the Model Ellipsoid and Normalized to Calculated Values Using the Adapted Model at Different ASR and NaCl Contents; Simultaneous Orientated Films; D(v, 0.5) of NaCl 30.1 μm ; (Ideal Model: Normalized Value Equals 1; Measured Value Equals Calculated Value)

ASR	2	4	9	25	
$V_{\text{headspace,measured}} \cdot V_{\text{headspace,model ellipsoid}}^{-1} [\text{cm}^3 \cdot \text{cm}^{-3}]$					
NaCl content in film [g NaCl·g film ⁻¹]	0.03	1.95 ± 0.01	1.50 ± 0.01	1.03 ± 0.01	0.78 ± 0.04
	0.06	1.48 ± 0.01	1.75 ± 0.01	0.80 ± 0.01	0.65 ± 0.05
	0.12	1.70 ± 0.01	1.21 ± 0.03	0.90 ± 0.03	0.59 ± 0.12
	0.24	2.17 ± 0.02	1.33 ± 0.02	0.81 ± 0.05	0.41 ± 0.22
$V_{\text{headspace,measured}} \cdot V_{\text{headspace,model adapted}}^{-1} [\text{cm}^3 \cdot \text{cm}^{-3}]$					
NaCl content in film [g NaCl·g film ⁻¹]	0.03	1.20	1.04	1.00	1.45
	0.06	0.83	1.22	0.76	1.20
	0.12	0.96	0.84	0.87	1.09
	0.24	1.22	0.92	0.78	0.77

Table IVb. Deviation of Data from Table IVa from Ideal Correlation of Model Ellipsoid and Adapted Model (Ideal Model: Deviation Equals Zero)

	ASR	2	4	9	25	
$ V_{\text{headspace,measured}} - V_{\text{headspace,model ellipsoid}}^{-1} [\text{cm}^3 \cdot \text{cm}^{-3}]$						∅
NaCl content in film [g NaCl·g film ⁻¹]	0.03	0.95	0.50	0.03	0.22	0.43
	0.06	0.48	0.75	0.20	0.35	0.45
	0.12	0.70	0.21	0.10	0.41	0.36
	0.24	1.17	0.33	0.19	0.59	0.57
	∅	0.83	0.45	0.13	0.39	0.45 ± 0.19
$ V_{\text{headspace,measured}} - V_{\text{headspace,model adapted}}^{-1} [\text{cm}^3 \cdot \text{cm}^{-3}]$						∅
NaCl content in film [g NaCl·g film ⁻¹]	0.03	0.20	0.04	0.00	0.45	0.18
	0.06	0.17	0.22	0.24	0.20	0.21
	0.12	0.04	0.16	0.13	0.09	0.11
	0.24	0.22	0.08	0.22	0.23	0.19
	∅	0.16	0.13	0.15	0.24	0.17 ± 0.06

oriented films were compared (Table V, Table VI). Biaxial-sequential orientation caused a slightly higher porosity than biaxial-simultaneous orientation. However, the results were not significant due to the overlapping confidence intervals. Porosities of biaxial-simultaneous and mono-axial oriented films were in the same confidence interval at SR and ASR of 2. At a SR and ASR of 4, biaxial-simultaneous orientation induced a slightly higher porosity, which were significant (confidence intervals not overlapping) at 6 g NaCl·g film⁻¹ and 24 g NaCl·g film⁻¹. This result can be attributed to the Poisson effect. The thinning, due axial orientation, is more important for higher SR. This is the case for mono-axial orientation compared to biaxial-simultaneous orientation when SR and ASR are equal. Nonetheless, the effect was not as clearly observable as expected. The approximations (eqs. 25 and 26) can be applied for biaxial-sequential and mono-axial orientated films, too. In the case of mono-axial orientation, ASR is equal to SR. Due to the Poisson effect, mono-axial orientation results in a slightly smaller porosity. The consequence for industrial processes is that different

orientation processes can be applied, yielding results that are of the same magnitude. The results furthermore confirm the finding that high porosity can be achieved by using a higher salt content or a higher SR.

Particle Size

Approximations (eqs. 25 and 26) are independent of particle size. However, particle size has an influence on gained porosities (Figure 10). Hence, eqs. (25) and (26) can be applied with acceptable results only for the tested medium particle sizes of 30–91 μm. Used NaCl powders had a distribution in particle size. Smaller particles contributed less to the porosity increase by orientation than bigger particles. For this reason, the correlation observed is an integration of effects of the particle size distribution of NaCl. The correlation needs to be further refined to successfully describe the influence of different uniform particle sizes.

In contrast to the present study, Nago et al. showed that a porosity of 67% v/v to 72% v/v can be achieved at low mean particle sizes of 0.08 μm to 3 μm.¹¹ In this case, PP films with

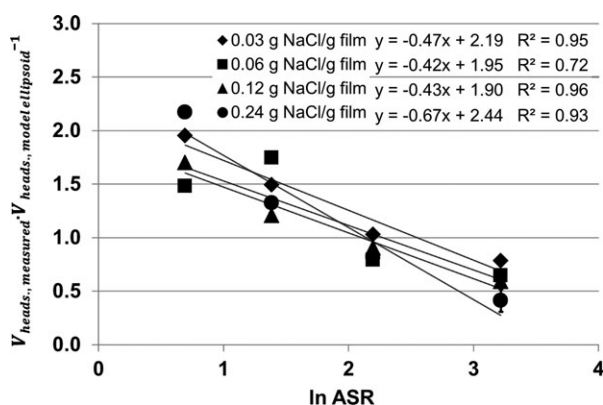


Figure 7. Quotient of headspace in capillaries calculated from density and using model ellipsoid as a function of the natural logarithm of ASR; biaxial-simultaneous oriented films; $D(v, 0.5)$ of NaCl 30.1 μm.⁵

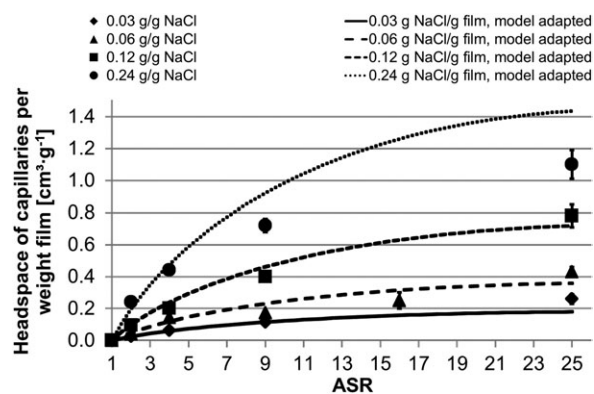


Figure 8. Headspace of capillaries per weight of film as a function of ASR; biaxial-simultaneous orientated films; $D(v, 0.5)$ of NaCl 30.1 μm; model adapted equation 25.⁵

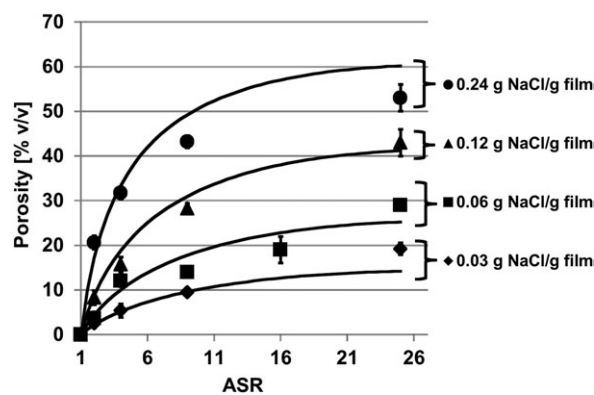


Figure 9. Porosity as a function of ASR; biaxial-simultaneous orientated films; $D(v, 0.5)$ of NaCl $30.1 \mu\text{m}$; model adapted equation 26.⁵

dispersed calcium carbonate powder at a concentration of 59% w/w were used. The films were stretched at a lower temperature of 90°C and a SR in machine direction of 2.8, and afterwards at 120°C and a SR in transversal direction of 1.8. Comparison of the results of the present study and of those of Nago et al. indicates that lower temperatures during stretching or high filler content may cause better capillary forming.

CONCLUSIONS

In this study, headspace-forming porosities of NaCl-filled PP films were correlated with SR and ASR. An empirically-adapted model based on ellipsoids allowed approximation of the correlation for a particle size of $30\text{--}91 \mu\text{m}$. The porosity increased with higher SR, ASR and higher NaCl content in films, respectively. The model can be applied for biaxial-simultaneous, biaxial-sequential and mono-axial-oriented films.

Table V. Porosity at Different ASR; Comparison of Biaxial-Simultaneous and Biaxial-Sequential Orientated Films; $0.06 \text{ g NaCl}\cdot\text{g film}^{-1}$; $D(v, 0.5)$ of NaCl $30.1 \mu\text{m}$

ASR	Porosity [% v/v]				
	2	4	9	16	25
Biaxial-simultaneous orientation	3.6 ± 1.5	12.0 ± 1.3	14.0 ± 0.7	19.0 ± 3.0	29.0 ± 1.1
Biaxial-sequential orientation	5.2 ± 1.3	9.0 ± 4.0	20.0 ± 4.0	25.0 ± 3.0	33.0 ± 3.0

Table VI. Porosity at Different SR and ASR; Comparison of Mono-Axial and Biaxial-Simultaneous Orientated Films; $D(v, 0.5)$ of NaCl $30.1 \mu\text{m}$

Salt content [g NaCl·g film ⁻¹]	Porosity [% v/v]			
	SR, ASR: 2		SR, ASR: 4	
	Monoaxial orientation	Biaxial-simultaneous orientation	Monoaxial orientation	Biaxial-simultaneous orientation
3	2.4 ± 1.2	2.5 ± 0.9	4.2 ± 1.4	5.4 ± 1.5
6	5.0 ± 3.0	3.6 ± 1.5	6.4 ± 1.8	12.0 ± 1.3
12	9.0 ± 3.0	8.3 ± 1.6	15.0 ± 3.0	15.7 ± 1.7
24	17.0 ± 8.0	20.6 ± 1.5	25.6 ± 1.8	31.7 ± 1.4

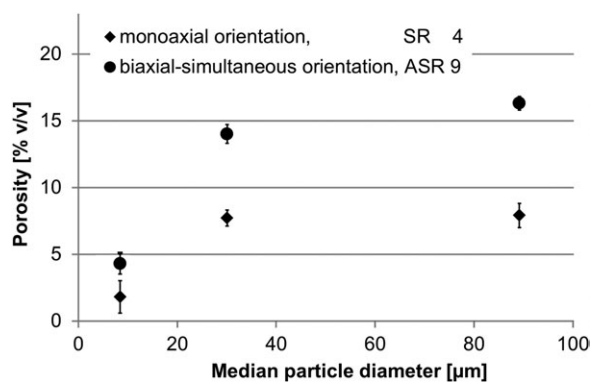


Figure 10. Porosity as a function of $D(v, 0.5)$ values of NaCl; $0.06 \text{ g NaCl}\cdot\text{g film}^{-1}$, SR 4

The model is independent of particle size. However, the present results showed that particle size has an influence on the porosity of oriented films. Therefore, the model needs to be optimized to include particle size. Nonetheless, the developed model is a useful approximation for medium particle sizes of $30\text{--}91 \mu\text{m}$.

The porosity of salt-loaded films correlated with their ability to bind water vapor. A porosity of 40% v/v is considered here to be a sufficient value achieved with $0.24 \text{ g NaCl}\cdot\text{g film}^{-1}$ at an ASR of 9 or with half the NaCl content of $0.12 \text{ g NaCl}\cdot\text{g film}^{-1}$ at an ASR of 25. For industrial applications a compromise must be found between maximum possible and applicable ASR and salt content in films.

The presented model provides a basis for other polymer-salt systems. In this case, however, the model needs to be verified and adapted to different polymer systems, which is currently subject of ongoing investigations. Further studies should be

conducted with spherical particles with a narrow particle size distribution. Different particle sizes should be tested for their influence on the porosity of oriented films. Poisson's ratio and the volume expansion at higher temperatures and respective contraction at lower temperatures should be correlated with porosity as a function of ASR.

ACKNOWLEDGMENTS

The authors thank the Fraunhofer-Gesellschaft zur Förderung der angewandten Forschung e.V., Munich for financing the project. We thank our colleagues Michael Schott for testing particle size distribution with the "Mastersizer" and providing devices for sieving of NaCl, Brigitte Seifert and Simone Drötboom for taking microscopic pictures, Tobias Brandner and Norbert Rodler for supervising extrusion experiments, and Eva Kirchhoff and Jonathan Beauchamp for conceptual support of the work. Furthermore we thank Gabriel-Chemie, Weitnau for providing master batches containing NaCl and LyondellBasell for providing PP for the experiments.

REFERENCES

- Singh, P.; Wani, A. A.; Saengerlaub, S. *Nutr. Food. Sci.* **2011**, *41*, 249.
- Sängerlaub, S.; Stramm, C. *Kunststoffe Int.* **2012**, 66–68.
- Langowski, H.-C.; Sängerlaub, S.; Wanner, T. (Fraunhofer-Gesellschaft zur Förderung der angewandten Forschung e.V.). Pat. WO/2007/121909, **2007**.
- Sängerlaub, S.; Böhmer, M.; Singh, P.; Stramm, C.; Langowski, H.-C.: In 13th European PLACE Conference **2011**, Bregenz, May 30–June 1, 2011; Vol. 2, 2011, 1228.
- Fraunhofer-Gesellschaft zur Förderung der angewandten Forschung e.V., internal results, **2012**.
- Wu, P. C.; Jones, G.; Shelley, C.; Woelfli, B. *J. Eng. Fiber Fabr.* **2007**, *2*, 49.
- Nagō, S.; Mizutani, Y. *J. Memb. Sci.* **1996**, *116*, 1.
- Nagō, S.; Mizutani, Y. *J. Appl. Polym. Sci.* **1995**, *56*, 253.
- Mizutani, Y.; Nagō, S. *J. Appl. Polym. Sci.* **1999**, *72*, 1489.
- Nagō, S.; Mizutani, Y. *J. Appl. Polym. Sci.* **1996**, *61*, 31.
- Nagō, S.; Nakamura, S.; Mizutani, Y. *J. Appl. Polym. Sci.* **1992**, *45*, 1527–1535.
- Kaufman, R. T.; Topolkaev, V., A.; Stopper, S. R.; Jacob, R. L. (Kimberly-Clark Worldwide, Inc.). Pat. WO/2008/027046, **2008**.
- Su, T. K.; Moreau, L.; Kitchin, K. (Toray Plastics America Inc.). *US Pat.* 6,855,411, **2005**.
- Larson, J. M. (Minnesota Mining and Manufacturing Company). Pat. WO/1997/000724, **1997**.
- Nakamura, S.; Kaneko, S.; Mizutani, Y. *J. Appl. Polym. Sci.* **1993**, *49*, 143.
- Nentwig, J. Ed. *Kunststoff-Folien, Herstellung-Eigenschaften-Anwendung*; Carl Hanser Verlag: München, **2006**; pp 74.
- Moore, E.P. In *Polypropylene Handbook*; Pasquini N., Eds.; Carl Hanser Verlag: München, **2005**; pp 310.
- Domininghaus, H. Ed. *Die Kunststoff und ihre Eigenschaften*. Springer-Verlag: Berlin, **1998**; pp 207–209.
- Van Krevelen, D. W. Ed. *Properties of Polymers*. Elsevier Science Publishing Company: Amsterdam, **1990**; pp 369.
- Elias, H.-G. Ed. *Makromoleküle Band 1*. Hüthig&Wepf Verlag: Basel, **1990**; pp 919.
- Saechtling, H.; Pabst, F. Eds. *Kunststoff Taschenbuch*. Carl Hanser Verlag: München, **1995**; pp 117.
- Anonymous. Product data sheet: esco Siede-Speisesalz Extrafine. Version 1.14. escoeuropean salt company: Hannover, Germany, **2007**.
- Hammond, C.R. In *CRC Handbook of Chemistry and Physics*; Lide, D. R., Ed.; CRC Press: Boca Raton, **1998**; pp 4.
- Stieß, M. Ed. *Mechanische Verfahrenstechnik*. Springer-Verlag: Berlin, Heidelberg, **1995**; pp 32.
- Anonymous. Product data sheet: Moplen HP525J, LyondellBasell, Rotterdam. The Netherlands, Release Date: 15 Jan 2008.
- Anonymous. Operating instructions: Density determination kit for Excellence XP/XS analytical balances, document number 11780508B – 0807/2.45, Mettler-Toledo AG, Greifensee, Switzerland, **2008**.
- Steel, R. G. D.; Torrie J. H., Eds. *Principles and Procedures of Statistics. A Biometric Approach*. Mc Graw-Hill: New York, **1980**.
- Grosche, G.; Beckmann, P., Eds. *Taschenbuch der Mathematik/I*. N. Bronstein; K.A. Semendjajew; Verlag Harri Deutsch: Thun and Frankfurt am Main, Germany, **1987**; pp 233.